

Energy and target dependence of projectile breakup effect in elastic scattering of ${}^6\text{Li}$

Y. Sakuragi*

Institute for Nuclear Study, University of Tokyo, Tanashi, Tokyo 188, Japan

(Received 1 December 1986)

For a wide range of incident energy ($E_{\text{lab}}=40\text{--}170$ MeV) and target mass number ($A=12\text{--}208$), projectile breakup effects in elastic scattering of ${}^6\text{Li}$ have been investigated in the microscopic coupled-channel framework; coupling with ${}^6\text{Li}\rightarrow\alpha+d$ breakup process is taken into account by the method of coupled discretized continuum channels. ${}^6\text{Li}$ -target interactions are provided by folding of the M3Y effective nucleon-nucleon potential with nucleon densities of colliding nuclei. The calculation reproduces well experimental data of elastic scattering for all the targets and incident energies investigated, without any renormalization of the folding real potential. The breakup effect is found to depend little on the energy and target, which is shown by calculating dynamical polarization potentials induced by the breakup process. The dynamical polarization potential has a repulsive real part with strength of about 40% of the folding potential, the imaginary part being negligible, which explains well the empirical reduction factor of the single-channel double-folding model. The origin of repulsive nature of the breakup effect is discussed.

I. INTRODUCTION

In recent years it has attracted considerable attention that projectile breakup processes are very important in considering scattering of light heavy ions, particularly of lithium isotopes, by nuclei.¹⁻⁹ The ground states and low-lying excited states of these isotopes have loosely bound cluster structures, i.e., ${}^6\text{Li}=\alpha+d$ and ${}^7\text{Li}=\alpha+t$, and the relative motion between the clusters are easily excited by external nuclear and/or Coulomb field of the target nucleus. Since excited states of ${}^6\text{Li}$ (${}^7\text{Li}$) at $E_x > 1.475$ MeV (2.468 MeV) are unbound against the decay into the clusters, excitations of those states lead to breakup of the projectile. The breakup may affect elastic scattering of the isotopes through virtual processes; i.e., the projectile virtually breaks up when it comes across the target nucleus and is deexcited to the ground state at the final stage of reaction. Those breakup effects are considered to be responsible for the famous anomaly¹⁰⁻¹⁶ of the renormalization factor ($N_R=0.5\text{--}0.6$) in the double folding (DF) model¹⁰ with the M3Y effective nucleon-nucleon (NN) potential¹⁷ in ${}^6,{}^7\text{Li}$ scattering. This has been discussed recently in theoretical studies of several groups.^{1-7,18} Significant effects of ${}^6\text{Li}\rightarrow\alpha+d$ breakup on elastic scattering were first demonstrated by Thompson and Nagarajan¹ (TN) for ${}^6\text{Li}$ scattering by ${}^{12}\text{C}$, ${}^{40}\text{Ca}$, and ${}^{208}\text{Pb}$ at $E_{\text{lab}}=156$ MeV. Since the method of TN was based on the adiabatic approximation¹⁹ for the breakup process and their interactions are essentially α -target and d -target optical potentials, the direct relation between the breakup effect and the anomalous reduction of N_R in the DF model was still obscure. However, the result of TN that well reproduced observed elastic scattering suggested that the breakup effect can be a reasonable candidate for the origin of $N_R=0.5\text{--}0.6$. In fact, Mackintosh and co-workers have shown by their potential inversion method that the breakup effects of the TN calculation are interpreted as additional repulsion to the real potential.¹⁸ One direct in-

dication of the relation between ${}^6\text{Li}$ breakup and the reduction of N_R was shown by Sakuragi, Yahiro, and Kamimura³ (SYK) on the basis of a microscopic version³ of the method of coupled discretized continuum channels (CDCC),²⁰⁻²³ in which the double folding interactions from the M3Y internucleon potential were employed for projectile-target interactions. In the work of SYK, observed elastic scattering of ${}^6\text{Li}$ by ${}^{28}\text{Si}$ at 99 MeV and that by ${}^{40}\text{Ca}$ at 156 MeV were reproduced well by the double folding interactions with $N_R=1.0$ when coupling with breakup channels was taken into account by the CDCC method; also calculated was the dynamical polarization (DP) potential³ induced by the coupling, which provided evidence of the relation mentioned above. A similar study has been reported by Gomez-Camacho *et al.*,⁷ where breakup effects were investigated in elastic scattering of ${}^6\text{Li}$ and ${}^7\text{Li}$ by ${}^{58}\text{Ni}$ for an energy range of 12-74 MeV.

To establish an understanding of the renormalization of the real DF interaction as the virtual breakup effect and to get more insight into the lithium-nucleus interaction, it may be necessary to extend the analyses of breakup effects over a wide range of bombarding energies and for many target nuclei. In light of these circumstances, this paper investigates ${}^6\text{Li}$ breakup effects on elastic scattering by the CDCC method of SYK in a systematic way over a wide range of bombarding energy (E_{lab}) and target mass number (A_T), say, $30 \leq E_{\text{lab}} \leq 170$ MeV and $12 \leq A_T \leq 208$, which almost cover the energy and target ranges of currently available data for elastic scattering of ${}^6\text{Li}$, and examines whether observed elastic scattering is reproduced by the double-folding interaction, with N_R fixed at unity, when coupling with the ${}^6\text{Li}$ breakup process is included by the CDCC calculation. The relation between the virtual breakup effect and the renormalization of the DF interaction without breakup is extensively studied from various viewpoints, as will be summarized below, for example, through breakup equivalent dynamical polarization potentials including the dependences on the incident

energy, target nucleus, and projectile angular momentum.

In the theoretical framework of SYK there is a single parameter N_I for the imaginary potential strength, as will be shown below, the value of which is determined in such a way that observed elastic-scattering cross sections are satisfactorily reproduced by the CDCC calculation. Good fits to the data with the single parameter N_I are not *a priori* guaranteed in this framework and, therefore, successful fits by the calculation are not artificial and rather should be taken to validate the theoretical framework. It should be noted that when coupling with breakup channels is omitted, the observed cross section cannot be fitted at all, not even by modifying the imaginary potential in the elastic channel. Furthermore, when the CDCC calculation is performed with *real coupling potentials alone*, observed data cannot be reproduced, as will be shown. Thus, the optimum value of N_I obtained by the CDCC fit to data and its energy and target dependences is expected to bear some information about basic interactions (or *bare potentials*) for the ${}^6\text{Li}$ -nucleus system and the reaction mechanism concerned.

In the next section we briefly summarize essential points of the method, i.e., the microscopic α -d cluster model description of ${}^6\text{Li}$ internal states, discretization of unbound continuum states, and coupled-channel equations including the discretized breakup channels. Double folding interactions are adopted for projectile-target diagonal potentials for all the channels, as well as for coupling potentials between the channels. In Sec. III the method is applied to ${}^6\text{Li}$ elastic scattering by ${}^{12}\text{C}$, ${}^{28}\text{Si}$, ${}^{40}\text{Ca}$, ${}^{48}\text{Ca}$, ${}^{58}\text{Ni}$, and ${}^{208}\text{Pb}$ at bombarding energies of $E_{\text{lab}} = 34\text{--}169$ MeV. The calculation reproduces well the measured cross sections for all the targets and bombarding energies *without* imposing any reduction factor to the real potential, i.e., keeping N_R at unity. The breakup effects are very large and are essential to reproduce the observed data. These results provide substantial evidence that the ${}^6\text{Li}$ breakup effect is the real origin of the reduction of N_R found in the single-channel DF-model analyses of ${}^6\text{Li}$ elastic scattering. Since the reduction of N_R was almost constant (0.5–0.6) over a wide range of bombarding energies and targets, this also implies that the breakup effect is almost independent of bombarding energy and target nucleus. However, the breakup effects behave in the angular distributions of elastic cross sections as if the effect would depend greatly on bombarding energy and target nucleus. The reason for such appearances will be explained by the decomposition of the scattering amplitude into contributions from nearside and farside scattering for typical cases. Improvements of fits at large angles in the highest energy scattering are also discussed in Sec. III. In Sec. IV dynamical polarization (DP) potentials induced by the coupling with breakup channels are calculated for several energies and targets. It is shown, almost independently of bombarding energy and target nucleus, that the coupling generates a repulsive real potential which cancels out, in the nuclear surface region, about 40% of the attractive potential obtained by the simple double folding of the M3Y interaction. In addition, the coupling causes little modification of the imaginary part of the ${}^6\text{Li}$ -target potential. These properties of DP potentials support the

above conjecture on the energy and target independence of the breakup effect. It is also shown that the real-to-imaginary ratio of the DP potential is quite sensitive to the strength of imaginary coupling potentials. In Sec. V the origin of the repulsive nature of the breakup effect is discussed. Based on perturbation theory, *explicit* relationships between the strengths of the DP and coupling potentials are derived, which clarifies a reason why the imaginary part of the coupling potentials is important in considering properties of the DP potential, such as the real-to-imaginary ratio. The final section is devoted to a summary of the results.

II. MICROSCOPIC COUPLED-CHANNEL FORMALISM

Full details of the microscopic coupled-channel formalism including treatment of ${}^6\text{Li}$ breakup states were described in Ref. 3. In this section we briefly summarize essential points of the method.

A. Microscopic α -d cluster model for ${}^6\text{Li}$

In the microscopic α -d cluster model, totally antisymmetrized wave functions are written as

$$\psi_{01+K}({}^6\text{Li}; \text{g.s.}) = \mathcal{A} \{ \phi(\alpha) [\phi_{1+}(\text{d}) \otimes u_{l=0}^{(1+)}(\mathbf{r})]_{1+K} \} \quad (2.1)$$

for the ground state, and

$$\psi_{lIK}({}^6\text{Li}; k) = \mathcal{A} \{ \phi(\alpha) [\phi_{1+}(\text{d}) \otimes u_l^{(l)}(k, \mathbf{r})]_{lK} \} \quad (2.2)$$

for the α -d scattering state with the asymptotic momentum $\hbar k$. Here, $\phi(\alpha)$ and $\phi_{1+}(\text{d})$ are internal wave functions of alpha and deuteron clusters, and $u_l(\mathbf{r})$ represents the α -d relative motion with angular momentum $\hbar l$; \mathcal{A} stands for the total antisymmetrization operator among six nucleons. The ground state is assumed to be a pure S state ($l=0$).

$u_m^{(l)}$ is assumed to satisfy an integrodifferential equation of an orthogonality condition model (OCM),²⁴

$$\sqrt{1-\mathcal{K}} \left[-\frac{\hbar^2}{2\mu_r} \nabla^2 + V_{\text{eff}} + \alpha_{l,l} V_{\text{eff}}^{(\text{so})} - \epsilon \right] \sqrt{1-\mathcal{K}} u_m^{(l)} = 0, \quad (2.3)$$

which is known to be a good approximation of the resonating group method (RGM).²⁵ Here, ϵ is the α -d c.m. energy and μ_r is the reduced mass of the α -d system; \mathcal{K} is the exchange-overlap kernel. The local potentials $V_{\text{eff}}(r)$ and $V_{\text{eff}}^{(\text{so})}(r)$ are the effective central and spin-orbit potentials, which are functions of the α -d relative distance r and are parametrized by a two-range Gaussian form for the central part and by a two-range Gaussian derivative form for the spin-orbit part, respectively.³ $\alpha_{l,l}$ stands for

$$[I(I+1) - l(l+1) - 1(1+1)]/2.$$

Since our aim here is just to prepare reliable internal wave functions of ${}^6\text{Li}$, we choose the potential parameters to be l dependent in such a way that the energy of the ground state ($\epsilon = -1.47$ MeV) (with respect to the α -d threshold),

and that of the 3^+ resonance state ($\epsilon=0.71$ MeV) and the α -d scattering phase shifts for each partial wave, are reproduced satisfactorily.³ The parameter values obtained were given in Ref. 3.

The microscopic wave functions are obtained by inserting $u_{lm}^{(J)}$, the solution of Eq. (2.3), into Eqs. (2.1) and (2.2). The wave functions of the ground and 3^+ -resonance states reproduce well the elastic and inelastic ($1^+ \rightarrow 3^+$) electron-scattering form factors. The calculated value of the rms charge radius of the ground state is 2.58 fm and that of the $B(E2; 1^+ \rightarrow 3^+)$ strength is $27.8 e^2 \text{fm}^4$, which agrees well with empirical values²⁶ of 2.56 ± 0.05 fm and $21.8 \pm 4.8 e^2 \text{fm}^4$, respectively.

In the CDCC calculations shown below, we “switch off” $V_{\text{eff}}^{(\text{so})}$ in Eq. (2.3) to save the computational time; namely, we neglect deuteron spin after performing the examination of the wave functions described above and recalculate u_{lm} using only the central potentials (V_{eff}) with their parameters unchanged. The ground-state wave function is unchanged by this approximation, whereas the D -wave resonances (3^+ , 2^+ , and 1^+) become degenerate at

$\epsilon \approx 2$ MeV with a width of about 1 MeV. The neglect of deuteron spin greatly reduces the computational time for the CDCC calculation of ${}^6\text{Li}$ scattering, while final results of the calculation differ little from those obtained by the calculation with deuteron spin. To simplify the formulas in this approximation, we introduce the following new notations:

$$\psi_{00}({}^6\text{Li}; \text{g.s.}) = \mathcal{A}[\phi(\alpha)\phi(d)u_{00}(\mathbf{r})], \quad (2.4)$$

for the ground state ($l=m=0$) wave function, and

$$\psi_{lm}({}^6\text{Li}; k) = \mathcal{A}[\phi(\alpha)\phi(d)u_{lm}(k, \mathbf{r})] \quad (2.5)$$

for the scattering state wave function with angular momentum $\hbar l$ and momentum $\hbar k$.

B. Discretization of the α -d continuum

The total wave function of the ${}^6\text{Li}$ -target system with total angular momentum J and its z component M is expanded in terms of the ${}^6\text{Li}$ internal-state wave functions as

$$\Psi_{JM} = \left\{ \psi_{00}({}^6\text{Li}; \text{g.s.}) \chi_{0J}^{(J)}(\hat{P}_0, \mathbf{R}) + \sum_{l=0}^{l_{\text{max}}} \sum_L \int_0^{k_{\text{max}}} [\psi_l({}^6\text{Li}, k) \otimes \chi_{lL}^{(J)}(P_k, \mathbf{R})]_{JM} dk \right\} \Phi_0^{(T)}, \quad (2.6)$$

where $\hbar L$ is the orbital angular momentum ($|J-l| \leq L \leq J+l$) between projectile and target. $\Phi_0^{(T)}$ stands for the ground-state wave function of target nucleus. In the equation, l_{max} and k_{max} are introduced to truncate the three-body model space.²⁰⁻²³ The wave functions $\chi_{0J}^{(J)}(\hat{P}_0, \mathbf{R})$ and $\chi_{lL}^{(J)}(P_k, \mathbf{R})$ describe ${}^6\text{Li}$ -target relative motions in the incident and breakup channels, respectively. $\hbar\hat{P}_0$ and $\hbar\hat{P}_k$ are the asymptotic momenta of the relative motion in the corresponding channels.

The truncated k continuum in Eq. (2.6) is divided into a finite number of narrow bins as $[k_{i-1}, k_i]$ ($i=1-N$) with $k_0=0$ and $k_N=k_{\text{max}}$. Though N could depend on l , we drop the suffix l for simplicity of notation. For each bin, any $\chi_{lL}^{(J)}(P_k, \mathbf{R})$ within the bin is assumed to be proportional to $\chi_{lL}^{(J)}(\hat{P}_i, \mathbf{R})$ with a proportional constant $f_{il}(k)$ which is a function of k ,

$$\chi_{lL}^{(J)}(P_k, \mathbf{R}) \approx f_{il}(k) \chi_{lL}^{(J)}(\hat{P}_i, \mathbf{R}). \quad (2.7)$$

Here, $\hbar\hat{P}_i$ is the ${}^6\text{Li}$ -target relative momentum associated with a mean energy³ $\hat{\epsilon}_i$ of the i th interval $[k_{i-1}, k_i]$. For a “nonresonant” bin where no α -d resonance exists, we take $f_{il}(k)=1$, which implies that we assume that the relative motion between ${}^6\text{Li}$ and target may not change so much with k within the interval. This may be a reasonable assumption when the interval is sufficiently small. For a “resonance” bin in which an α -d resonance with width Γ exists at $\epsilon = \epsilon_{\text{res}}$, we take

$$f_{il}(k) = |(i\Gamma/2)/(\epsilon_k - \hat{\epsilon}_i + i\Gamma/2)|,$$

where $\hat{\epsilon}_i = \epsilon_{\text{res}}$. Under the assumption of Eq. (2.7), the total wave function is written as

$$\Psi_{JM} = \sum_{l=0}^{l_{\text{max}}} \sum_L \sum_{i=0 \text{ or } 1}^N [\hat{\psi}_{il}({}^6\text{Li}) \otimes \chi_{ilL}^{(J)}(\mathbf{R})]_{JM} \Phi_0^{(T)}, \quad (2.8)$$

with

$$\hat{\psi}_{ilm}({}^6\text{Li}) = (1/\sqrt{N_{il}}) \int_{k_{i-1}}^{k_i} \psi_{lm}({}^6\text{Li}, k) f_{il}(k) dk, \quad (2.9)$$

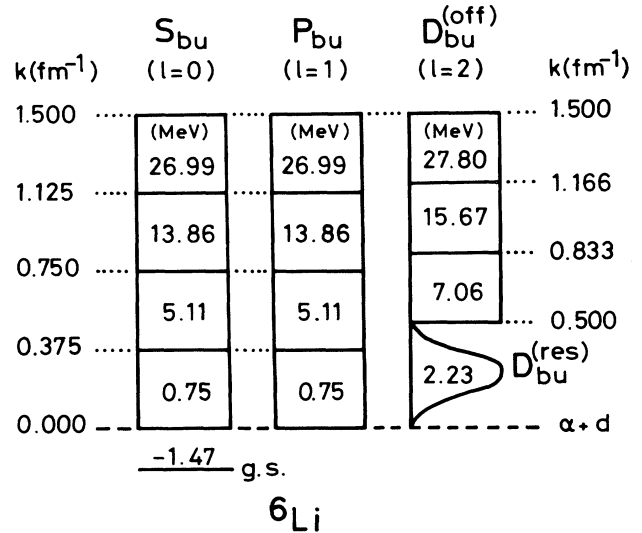


FIG. 1. Truncation and discretization of the α -d breakup continuum of ${}^6\text{Li}$. Here, the spin-orbit potential between α and d , $V_{\text{eff}}^{(\text{so})}$, has been switched off. The number in each box is the mean energy of the bin. The lowest bin of the D wave ($l=2$) stands for the resonance and the rest are the nonresonant continua.

$$\hat{\chi}_{iL}^{(J)}(\mathbf{R}) = \sqrt{N_{iL}} \chi_{iL}^{(J)}(\hat{P}_i, \mathbf{R}), \quad (2.10)$$

$$N_{iL} = \int_{k_{i-1}}^{k_i} [f_{iL}(k)]^2 dk, \quad (2.11)$$

where new notations,

$$\hat{\psi}_{i=0, l=0}({}^6\text{Li}) \equiv \psi_{l=0}({}^6\text{Li}; \text{g.s.})$$

and

$$\hat{\chi}_{i=0, l=0, L}^{(J)}(\mathbf{R}) \equiv \chi_{i=0, L}^{(J)}(\hat{P}_0, \mathbf{R})$$

have been used for the incident channel. The summation over i in Eq. (2.8) includes $i=0$ only when $l=0$.

In practical CDCC calculations of ${}^6\text{Li}$ scattering by target nucleus, we take $l_{\max}=2$ (S , P , and D waves), $N=4$,

and $k_{\max}=1.5 \text{ fm}^{-1}$. These values have been examined in Ref. 3 and were found to be sufficient for reasonable convergence of calculated cross sections as well as for S -matrix elements of elastic scattering. The discretized model space adopted here is illustrated in Fig. 1, where the lowest bin of the D wave ($l=2$) is the resonance bin mentioned above and the rest are the nonresonant bins.

C. CDCC equations with double-folding interaction

Now we introduce the radial wave function $\hat{\chi}_{iL}^{(J)}(R)$ by

$$\hat{\chi}_{iLM}^{(J)}(\mathbf{R}) \equiv \hat{\chi}_{iL}^{(J)}(R) i^L Y_{LM}(\hat{\mathbf{R}}) / R. \quad (2.12)$$

The coupled-channel (CC) equations (which we call the CDCC equations) for $\chi_{iL}^{(J)}(R)$'s are now written as

$$\left[-\frac{\hbar^2 d^2}{2\mu dR^2} + \frac{\hbar^2 L(L+1)}{2\mu R^2} + V_{\text{Coul}}(R) - (E - \hat{\epsilon}_i) \right] \hat{\chi}_{iL}^{(J)}(R) = - \sum_{i'l'L'} (N_R + iN_I) \hat{V}_{iL, i'l'L'}^{(J)}(R) \hat{\chi}_{i'l'L'}^{(J)}(R). \quad (i=0-N, l=0-l_{\max}, |J-l| \leq L \leq J+l). \quad (2.13)$$

The real part of the ${}^6\text{Li}$ -target potentials, $\hat{V}_{iL, i'l'L'}^{(J)}(R)$, is obtained by doubly folding an effective nucleon-nucleon (NN) interaction, v_{NN} , with the nucleon density distributions of the target and ${}^6\text{Li}$:

$$\begin{aligned} \hat{V}_{iL, i'l'L'}^{(J)}(R) &= \langle \Phi_0^{(T)} [i^l \hat{\psi}_{iL}({}^6\text{Li}) \otimes i^L Y_L(\hat{\mathbf{R}})]_{JM} | \sum_{\substack{i \in \text{Li} \\ j \in T}} v_{\text{NN}}(\mathbf{r}_i + \mathbf{R} - \mathbf{r}_j) | \Phi_0^{(T)} [i^{l'} \hat{\psi}_{i'l'}({}^6\text{Li}) \otimes i^{L'} Y_{L'}(\hat{\mathbf{R}})]_{JM} \rangle \\ &= \sum_{\substack{m, \mu \\ m', \mu'}} (lmL\mu | JM)(l'm'L'\mu' | JM) i^{L'+L-L-1} \int Y_{L\mu}^*(\hat{\mathbf{R}}) \hat{V}_{ilm, i'l'm'}(\mathbf{R}) Y_{L'\mu'}(\hat{\mathbf{R}}) d\hat{\mathbf{R}}, \end{aligned} \quad (2.14)$$

where

$$\begin{aligned} \hat{V}_{ilm, i'l'm'}(\mathbf{R}) &= \int \rho_T(\mathbf{r}_T) \hat{\rho}_{ilm, i'l'm'}(\mathbf{r}_P) \\ &\quad \times v_{\text{NN}}(\mathbf{r}_P + \mathbf{R} - \mathbf{r}_T) d\mathbf{r}_P d\mathbf{r}_T. \end{aligned} \quad (2.15)$$

Here, $\rho_T(\mathbf{r}_T)$ is the ground-state nucleon density of target nucleus with mass number A , which is defined as

$$\rho_T(\mathbf{r}_T) = \left\langle \Phi_0^{(T)} \left| \sum_{j=0}^A \delta(\mathbf{r}_j - \mathbf{r}_T) \right| \Phi_0^{(T)} \right\rangle, \quad (2.16)$$

and $\hat{\rho}_{ilm, i'l'm'}(\mathbf{r}_P)$ is the ${}^6\text{Li}$ density between the states $\hat{\psi}_{ilm}({}^6\text{Li})$ and $\hat{\psi}_{i'l'm'}({}^6\text{Li})$, which is calculated with the use of the ${}^6\text{Li}$ wave functions obtained above as

$$\hat{\rho}_{ilm, i'l'm'}(\mathbf{r}_P) = \left\langle \hat{\psi}_{ilm}({}^6\text{Li}) \left| \sum_{j=1}^6 \delta(\mathbf{r}_j - \mathbf{r}_P) \right| \hat{\psi}_{i'l'm'}({}^6\text{Li}) \right\rangle. \quad (2.17)$$

In this paper we analyze elastic scattering of ${}^6\text{Li}$ by ${}^{12}\text{C}$, ${}^{28}\text{Si}$, ${}^{40}\text{Ca}$, ${}^{48}\text{Ca}$, ${}^{58}\text{Ni}$, and ${}^{208}\text{Pb}$. The ground-state nucleon densities of ${}^{28}\text{Si}$, ${}^{40}\text{Ca}$, and ${}^{58}\text{Ni}$ are taken to be the same as those adopted in the double-folding model study of Ref. 11, whereas Hartree-Fock densities²⁷ are adopted for ${}^{48}\text{Ca}$ and ${}^{208}\text{Pb}$. As for ${}^{12}\text{C}$, we use the density calculated with the 3α -RGM wave function.²⁸ All these densities have been examined as to whether they could reproduce the observed electron-scattering form factors and the

rms radii.

As for the effective nucleon-nucleon interaction, v_{NN} , we use the spin- and isospin-singlet ($S=T=0$) components of the M3Y interaction¹⁷ with a pseudopotential which simulates the contribution from single-nucleon knock-on exchange.¹⁰ The explicit form is

$$v_{\text{NN}}(\mathbf{r}) = 7999 \frac{e^{-4r}}{4r} - 2134 \frac{e^{2.5r}}{2.5r} - \hat{J}_{00} \delta(\mathbf{r}), \quad (2.18)$$

where all energies are given in MeV and lengths in fm. The strength \hat{J}_{00} of the pseudopotential varies with bombarding energy,¹⁰ but the variation is small (less than 7% in volume-integral value) over the energy range $E/A_p = 5-30$ MeV (A_p being projectile mass number) of interest here. Therefore, we ignore the energy dependence and use a fixed value of $\hat{J}_{00} = 262 \text{ MeV fm}^3$, which is evaluated at $E/A_p = 10 \text{ MeV}$.¹⁰

In Eq. (2.13), N_R is kept fixed at unity throughout the CDCC calculation. On the other hand, the imaginary part of the diagonal and coupling potentials is simply assumed to have the same geometry as that of the corresponding real part. N_I is the strength factor of the imaginary part, which is taken to be common to all the potentials in the CDCC equations. Since the projectile breakup processes are peripheral phenomena,³ especially for heavy ions, the present assumption for imaginary potentials may be sufficient for discussions about essential features of breakup effects on elastic scattering. In this paper we do

not intend to clarify the origin of the imaginary part; instead, we determine the strength of the part N_I phenomenologically, for each scattering datum, in such a way that the CDCC calculation reproduces the observed cross section for the elastic scattering. It should be stressed that N_I is the single parameter in the present theoretical frame.

Projectile breakup by Coulomb interaction is ignored here for simplicity. The usual Coulomb potential $V_{\text{Coul}}(R)$ for the uniform-charge-density shape with a radius $R_C = 1.2(6^{1/3} + A^{1/3})$ fm is assumed commonly for all the channels in Eq. (2.13). Effects of Coulomb breakup on elastic scattering are expected not to be significant, except at low incident energies comparable with Coulomb barrier height.

The single-channel case of the present CDCC framework corresponds to the case of $N_R = 1$ of the DF model in which the imaginary potential shape is taken to be the same as that of the folding real potential, although a more flexible shape is allowed to be used in the DF model. Thus, it is possible to discuss direct relations between projectile breakup effects and the reduction of N_R from 1.0 to 0.5–0.6 in the DF model.

III. RESULTS

A. Coupled-channel calculations

Coupled-channel calculations including the breakup channels of Fig. 1 (which we call CDCC calculations)

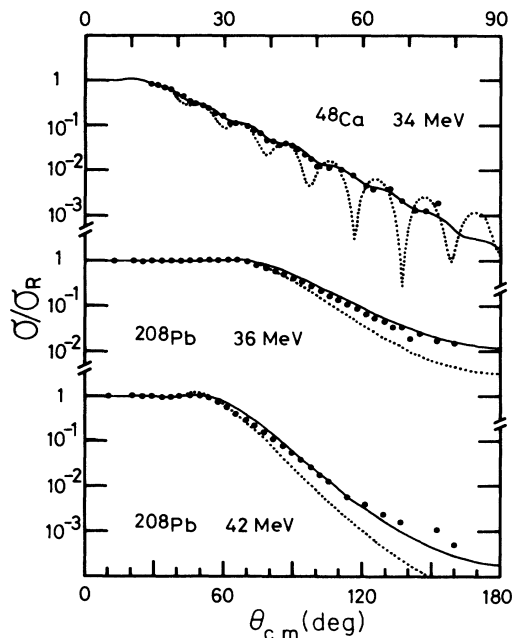


FIG. 2. Angular distributions of the elastic scattering of ${}^6\text{Li}$ by ${}^{48}\text{Ca}$ at $E_{\text{lab}} = 34$ MeV and by ${}^{208}\text{Pb}$ at 36 and 42 MeV. The upper angular scale is only for ${}^{48}\text{Ca}$ target and the lower scale for the others. The solid and the dotted lines show the results of the CDCC calculation and the single-channel one, respectively, with N_R kept fixed at unity. The experimental data are taken from Refs. 30 and 31.

have been performed for ${}^6\text{Li}$ scattering by ${}^{12}\text{C}$ at 50.6, 99, 123.5, 156, and 168.6 MeV, by ${}^{28}\text{Si}$ at 46, 99, 135, and 154 MeV, by ${}^{40}\text{Ca}$ at 50.6, 88, 99, and 156 MeV, by ${}^{48}\text{Ca}$ at 34 MeV, by ${}^{58}\text{Ni}$ at 50.6, 73.7, and 99 MeV, and by ${}^{208}\text{Pb}$ at 36, 42, 50.6, 73.7, 88, 99, and 156 MeV. The calculated elastic cross sections are grouped according to bombarding energy and shown by the solid lines in Figs. 2–7. In general, the CDCC calculation with $N_R = 1$ successfully reproduces the experimental data^{11,29–39} for all the targets and bombarding energies investigated here. These results imply that the projectile breakup effect accounts well for the reduction factor of $N_R = 0.5$ – 0.6 required in the single-channel DF-model studies of ${}^6\text{Li}$ scattering. Going into details, a fit to the data for ${}^{40}\text{Ca}$ at 88 MeV is exceptionally poor, which may, however, be due to an uncertainty of experimental data since these data were known to have suffered from some experimental difficulties.³⁹ For the higher energy cases in Figs. 6 and 7, pronounced deviations of the calculation from the data are observed at large angles, which may be due to a rather crude assumption for the imaginary potential in Eq. (2.13), since, at higher energies, cross sections at large angles are sensitive to details of the potential at the nuclear interior. An improvement of fits at those angles will be discussed later.

Listed in Table I are the optimum values of N_I deduced from the fit to experimental data with the CDCC calculation. No significant dependence on energy and target is seen, although smaller values ($N_I = 0.4$ – 0.5) are required for ${}^{12}\text{C}$ and ${}^{48}\text{Ca}$ targets and for low energy data on the ${}^{208}\text{Pb}$ target. For ${}^{208}\text{Pb}$ one should not take the small values of N_I at low energies seriously, since the fit to the

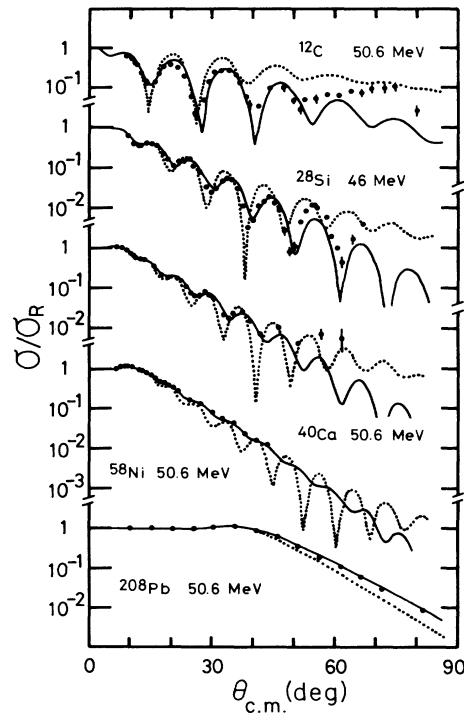


FIG. 3. The same as Fig. 2 for ${}^6\text{Li}$ scattering by ${}^{12}\text{C}$, ${}^{48}\text{Ca}$, ${}^{58}\text{Ni}$, and ${}^{208}\text{Pb}$ at 50.6 MeV and by ${}^{28}\text{Si}$ at 46 MeV. The data are taken from Refs. 13 and 32.

TABLE I. Optimum values of N_R and N_I for the CDCC calculations, the value of N_R being fixed at unity for all cases. J_{gr} is the grazing angular momentum for each scattering.

Target	E_{lab} (MeV)	N_R	N_I	J_{gr} (\hbar)	
^{12}C	50.6	1.00	0.50	11	
	99	1.00	0.50	15	
	123.5	1.00	0.48	18	
	156	1.00	0.47	20	
	168.6	1.00	0.47	21	
^{28}Si	46	1.00	0.62	14	
	99	1.00	0.62	23	
	135	1.00	0.65	27	
	154	1.00	0.59	29	
^{40}Ca	50.6	1.00	0.60	17	
	88	1.00	0.60	24	
	99	1.00	0.64	26	
	156	1.00	0.68	33	
^{48}Ca	34	1.00	0.50	14	
	^{58}Ni	50.6	1.00	0.60	19
		73.7	1.00	0.60	25
99		1.00	0.60	30	
^{208}Pb	36	1.00	0.40	8	
	42	1.00	0.40	13	
	50.6	1.00	0.60	18	
	73.7	1.00	0.62	29	
	88	1.00	0.60	35	
	99	1.00	0.62	38	
	156	1.00	0.60	53	

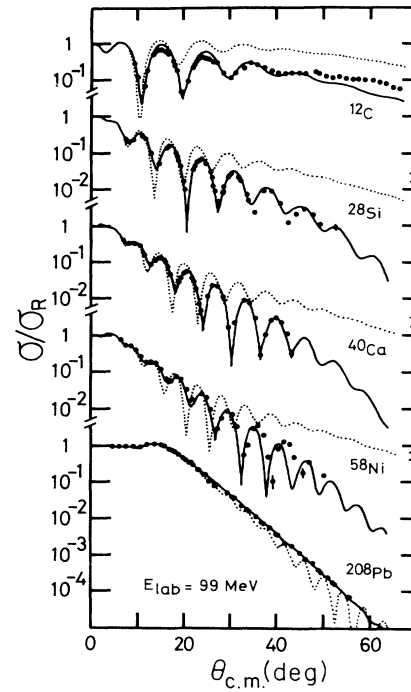


FIG. 5. The same as Fig. 2 for 99 MeV ^6Li scattering by ^{12}C , ^{28}Si , ^{40}Ca , ^{58}Ni , and ^{208}Pb . The data are taken from Ref. 11.

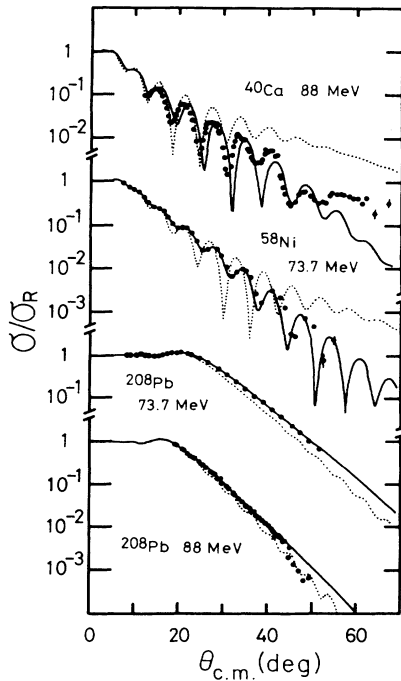


FIG. 4. The same as Fig. 2 for ^6Li scattering by ^{40}Ca and ^{208}Pb at 88 MeV and by ^{58}Ni and ^{208}Pb at 73.7 MeV. The data are taken from Refs. 33 and 34.

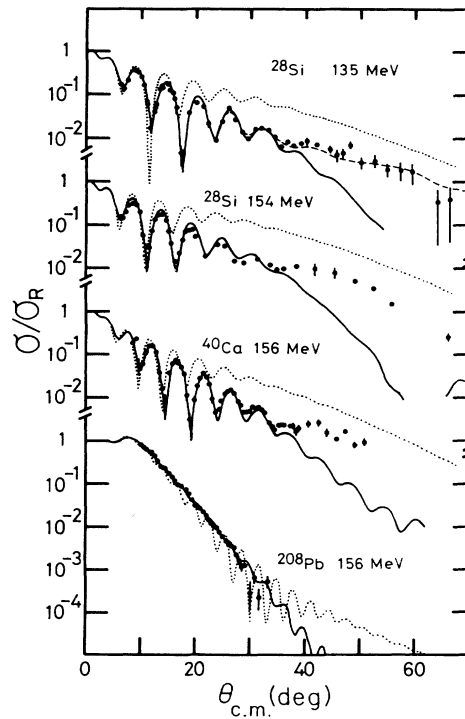


FIG. 6. The same as Fig. 2 for ^6Li scattering by ^{28}Si at 135 and 154 MeV and by ^{58}Ni and ^{208}Pb at 156 MeV. The data are taken from Refs. 35–38.

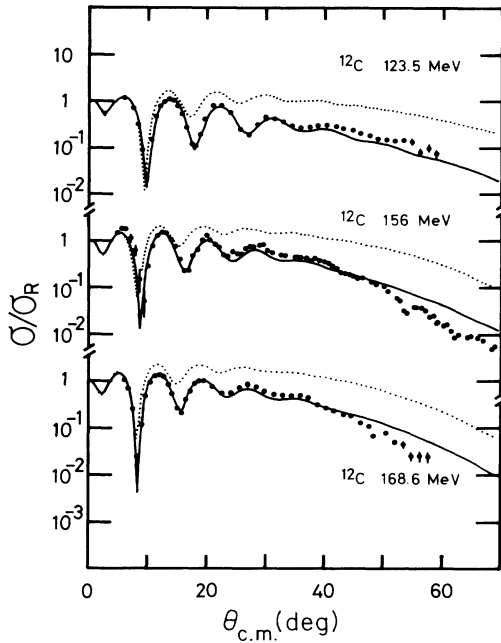


FIG. 7. The same as Fig. 2 for ^6Li scattering by ^{12}C at 123.5, 156, and 168.6 MeV. The data are taken from Refs. 29 and 38.

data is not perfect around grazing angles that may be due to neglect of Coulomb excitation effects in the calculation. Namely, those bombarding energies are comparable with Coulomb-barrier height for the ^6Li - ^{208}Pb system and considerable effects, e.g., long-range absorption, will be expected from the Coulomb excitation of the projectile by the target, which has been neglected in the present calculation.

The dotted lines in Figs. 2–7 show the result of a single-channel calculation using the same values of N_R ($=1$) and N_I as those for the corresponding CDCC calculation. Significant effects of breakup channels on elastic scattering are seen by the differences between the dotted and solid lines. It is known³ that a large fraction of the difference stems from the coupling to the D -wave resonance channel, although non-negligible contributions arise from the nonresonant breakup channels. It should also be stressed that couplings *among* the breakup channels are quite important for proper estimation of the breakup effects.³

Upon a first examination of Figs. 2–7, one might consider that the breakup effect on elastic scattering varies greatly with bombarding energy and target nucleus. For light targets, for which the angular distribution shows the Fraunhofer diffraction pattern, the breakup effect reduces the cross section from dotted lines to solid ones, while for heavy targets—the angular distribution being of the Fresnel type—the cross section increases with the breakup effect. However, for both targets the cross sections reflect the repulsive nature of the breakup effect, which can be understood naturally with *nearside/farside* (N/F) decomposition of scattering amplitudes,^{40,41} as shown below.

B. Nearside/farside decomposition

Following Ref. 40, we decompose the amplitude for elastic scattering, $f(\theta)$, into components of nearside and farside scattering,

$$f(\theta) = f_N(\theta) + f_F(\theta), \quad (3.1)$$

where each of $f_N(\theta)$ and $f_F(\theta)$ is composed of the Coulomb part and the nuclear part, respectively, as

$$f_N(\theta) = f_N^{(\text{Coul})}(\theta) + f_N^{(\text{nucl})}(\theta), \quad (3.2)$$

$$f_F(\theta) = f_F^{(\text{Coul})}(\theta) + f_F^{(\text{nucl})}(\theta). \quad (3.3)$$

Here, $f_N^{(\text{Coul})}(\theta)$ [$f_F^{(\text{Coul})}(\theta)$] is the nearside (farside) component of the Coulomb scattering amplitude, which is expressed with analytic functions.⁴⁰ The nuclear part of the nearside and farside components is expressed with the calculated S -matrix elements for elastic scattering, S_L , as

$$f_{N,F}^{(\text{nucl})}(\theta) = \frac{i}{2k} \sum_L (2L+1) \times \exp(2i\sigma_L^{(\text{C})})(1-S_L)Q_L^{(\pm)}(\cos\theta), \quad (3.4)$$

where $Q_L^{(+)}$ ($Q_L^{(-)}$) is the nearside (farside) component of the Legendre polynomial,⁴⁰ and $\sigma_L^{(\text{C})}$ is the Coulomb phase shift.

Figures 8(a) and 8(b) show the N/F decomposition of the scattering of ^6Li by ^{28}Si and ^{208}Pb at 99 MeV. Both the single-channel and CDCC result have been decomposed, where S_L in Eq. (3.4) is given by the single-channel and CDCC calculation, respectively. The dotted and dashed lines show individual contributions from the nearside and farside scattering, respectively, and the solid line shows their coherent sum. In the single-channel case for the ^{28}Si target, the *Fraunhofer crossover*⁴¹ between the nearside and farside occurs around $\theta_{c.m.} \simeq 15^\circ$ and the farside dominates the scattering for angles larger than the crossover point, which is called the *farside tail*.⁴¹ The tail has been reduced in the CDCC calculation. Hence, the decrease of the cross section for those angles from the single channel to the CDCC, as seen in Fig. 5 for the ^{28}Si target, is now understood as the result of the decrease of the farside tail. Conversely, the nearside component increases by the breakup effect, which leads to strong interference between the nearside and farside scattering over a wide range of angles around the crossover point, the coherent sum of which (solid line) reproduces the experimental data very well. For the ^{208}Pb target, the breakup effect also causes an increase (decrease) in the nearside (farside) component. However, the scattering by the target is dominated by the nearside for most angles of interest here, which is due to the strong Coulomb repulsion.⁴¹ Thus one may understand why the breakup effect causes the increase of cross section as well as the damping of oscillations at large angles for this target, as seen in Fig. 5.

Since an attractive real potential plays the role of a converging lens, a reduction of attractive potential strength causes a decrease of the farside amplitude and an increase

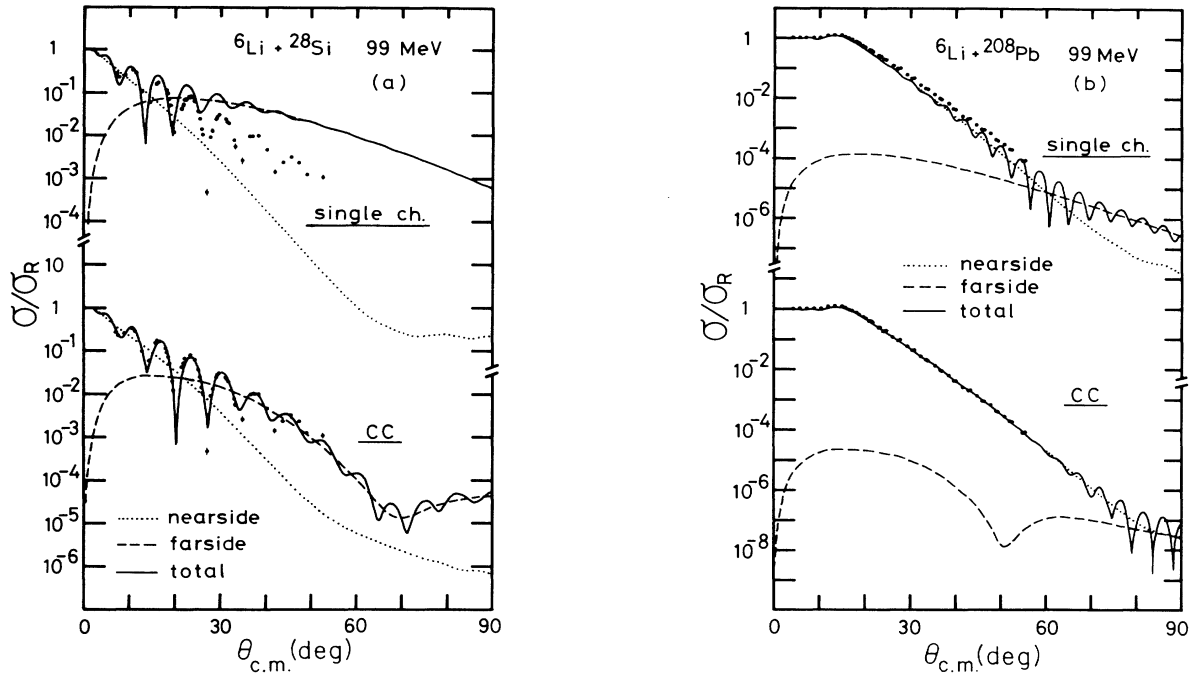


FIG. 8. The nearside/farside decomposition of the calculated ${}^6\text{Li}$ scattering (a) by the ${}^{28}\text{Si}$ target and (b) the ${}^{208}\text{Pb}$ target at 99 MeV; both the single-channel result (upper) and the CDCC one (lower) are decomposed into the nearside component (dotted lines) and the farside one (dashed lines); the coherent sum of them is shown by the solid lines.

of the nearside amplitude.⁴¹ Therefore, both the decrease of the farside-dominant cross section for the ${}^{28}\text{Si}$ target and the increase of the nearside-dominant one for the ${}^{208}\text{Pb}$ target in Figs. 8(a) and 8(b) reflect a reduction of attractive (real) potential strength by the breakup effect. In fact, the results of the CDCC calculation can be simulated well³ by a single-channel calculation with the DF potential multiplied by a factor ($N_R=0.5-0.6$), which is well known as the anomalous renormalization factor in the single-channel DF model for ${}^6\text{Li}$ scattering.¹⁰⁻¹⁶

With the above consideration kept in mind, one may easily understand that, for other targets and/or bombarding energies in Figs. 2-7, the change in the cross section from the dotted to solid line reflects the repulsive nature of the breakup effect.

C. Improvement of fits at higher-energy scattering

At higher incident energies, fits to experimental data at large angles are rather poor (see Figs. 6 and 7), even with including the breakup effect in the CDCC calculation, although large effects of breakup channels are still evident. In the present theoretical framework we have simply assumed the geometrical form of the imaginary potentials to be the same as that of the corresponding real potentials [cf. Eq. (2.13)]. As shown above, this assumption has been sufficient for discussions about the significant effects of breakup channels. However, this may be somewhat too simple to get excellent fits up to the large angles in high-energy scattering. At those energies, cross sections at large angles are very sensitive to details of the potential at the nuclear interior, which is indeed supported by the fact that observed large-angle scattering in Fig. 6 displays

nuclear-rainbow-like enhancements.¹³

It turns out that much better fits to the data at those angles are obtained with a modified CDCC calculation, the only difference from the previous calculation being that the imaginary potential in the incident channel is replaced by a phenomenological one with a Woods-Saxon shape, other potentials being unchanged. As will be shown in Sec. IV, the important effect of coupling with the breakup channels is production of a real potential of repulsive nature, and the contribution to the imaginary part is negligibly small. This repulsive effect of the coupling can be simulated simply by a renormalization of the real potential in the single-channel DF calculation by $N_R \simeq 0.6$. Thus it will be reasonable to limit the modification of the imaginary potential to the incident channel, keeping the breakup effect fixed, and to adopt the imaginary potential obtained by the single-channel DF-model fit to the elastic-scattering data as the new imaginary part.

The dashed line in Fig. 6 shows an example of such a modified CDCC calculation of the scattering by ${}^{28}\text{Si}$ at $E_{\text{lab}}=135$ MeV. The parameter values for the new imaginary potential are the following: $W_0=27.46$ MeV, $R_I=1.7A_T^{1/3}$ fm, where $A_T=28$, and $a_I=0.908$ fm, which have been obtained by the single-channel DF-model analysis of the same scattering.¹³

IV. DYNAMICAL POLARIZATION POTENTIAL

In order to confirm the repulsive nature of the breakup effect quantitatively, we calculate the dynamical polarization (DP) potential due to the breakup channels in the form of the wave-function-equivalent local potential. The real and imaginary parts of the potential are defined³ as

$$\Delta V^{(J)}(R) = \text{Re} \left[\sum_{i \neq 0} \sum_{iL} (N_R + iN_I) \hat{V}_{00J, iL}^{(J)} \hat{\chi}_{iL}^{(J)}(R) / \hat{\chi}_{00J}^{(J)}(R) \right] \quad (4.1)$$

and

$$\Delta W^{(J)}(R) = \text{Im} \left[\sum_{i \neq 0} \sum_{iL} (N_R + iN_I) \hat{V}_{00J, iL}^{(J)} \hat{\chi}_{iL}^{(J)}(R) / \hat{\chi}_{00J}^{(J)}(R) \right], \quad (4.2)$$

where N_R is kept fixed at unity and N_I is taken to be the optimum value for the corresponding CDCC calculation listed in Table I.

Before discussing the properties of the DP potential, it should be noted that in heavy-ion scattering like the present case elastic scattering is almost insensitive to the potential at the nuclear interior due to a strong absorptive potential, except for a few cases of high energy scattering discussed in the preceding section. As a measure useful for defining such an *insensitive region* in the nuclear interior, we adopt the change of the modulus of the elastic S -matrix element by less than 1% against the switching off of the DP potential in the region.³ In such an insensitive region, the modulus of the incident-channel wave function, $|\hat{\chi}_{00J}^{(J)}(R)|$, has been found empirically to be less than about 10% of its maximum value in the asymptotic region. Thus, we adopt the value of R satisfying the relation

$$|\hat{\chi}_{00J}^{(J)}(R)| \simeq 0.1 |\hat{\chi}_{00J}^{(J)}(\infty)|$$

as a measure for defining the insensitive region.

A. Angular momentum dependence

We first examine the angular-momentum dependence of the DP potential. In Fig. 9 we show the real and imaginary parts of the DP potential, $\Delta V^{(J)}$ and $\Delta W^{(J)}$, respectively, at the nuclear surface region in the case of $J=0, 10, 21, 25,$ and 28 of ${}^6\text{Li} + {}^{28}\text{Si}$ scattering at $E_{\text{lab}}=99$ MeV. The position of the boundary between the internal (insensitive) and peripheral regions depends on J , but we illustrate in Fig. 9 the boundary only for $J=21$ for simplicity; the approximate positions for other J 's are, for example, $R \simeq 4$ fm for $J=0$ and $R \simeq 6$ fm for $J=28$. Since the grazing angular momentum (J_{gr}) is 23 in the present case, the DP potentials for $J=0$ and 10 in the figure do not take part in the scattering at all, due to strong absorption, although we show them in the figure for comparison. The figure shows that the DP potential is almost independent of J around J_{gr} in the peripheral region. For such J , the potential really has a repulsive real part ($\Delta V^{(J)} > 0$) whose strength amounts to up to about 40% of the real DF potential, $V_{00}(R)$, of the incident channel. In other words, $V_{00}(R) + \Delta V^{(J)}(R)$ may almost l -independently be approximated well by $\sim 0.6V_{00}(R)$. This is just the origin of the reduction of N_R in the single-channel DF model for ${}^6\text{Li}$ scattering. The figure also shows that the imaginary part, $\Delta W^{(J)}$, is negligibly small in the peripheral region for J around J_{gr} . This property, $\Delta V > 0$ and $\Delta W \simeq 0$,

of the DP potential due to the breakup channels is completely different from that of the *familiar type* of the potential due to excitations of phononlike states of nuclei; the latter type of the potential is usually dominated by an absorptive imaginary part⁴² ($\Delta V \simeq 0, \Delta W < 0$). The existence of such a *new type* of DP potential has also been suggested in Refs. 3, 18, and 43.

B. Energy and target dependence

Secondly, we examine the incident-energy dependence of the DP potential. Since the potential is almost independent of J in the peripheral region, we calculate it for a specific J around J_{gr} for each incident energy. Figure 10 shows the real and imaginary parts of the DP potential for the scattering by ${}^{28}\text{Si}$ at $E_{\text{lab}}=46, 99,$ and 135 MeV

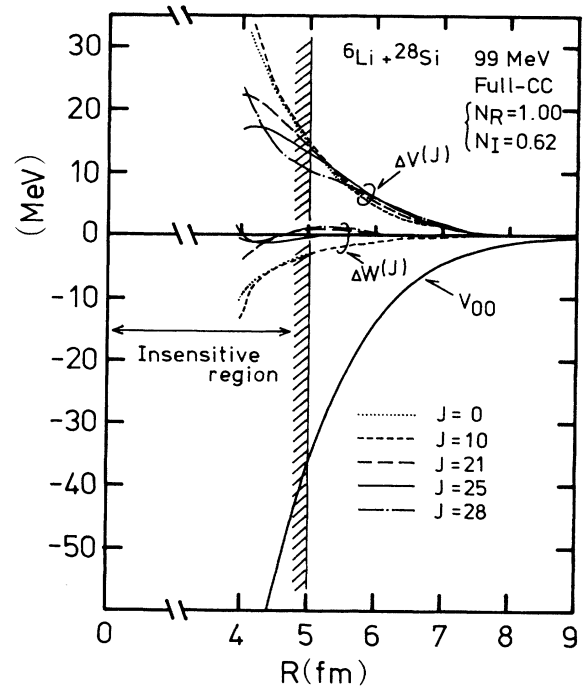


FIG. 9. Angular-momentum (J) dependence of the DP potential induced by the coupling with breakup channels for ${}^6\text{Li} + {}^{28}\text{Si}$ at 99 MeV. $\Delta V^{(J)}$ ($\Delta W^{(J)}$) is the real (imaginary) part of the potential for $J=0$ (dotted), 10 (short-dashed), 21 (long-dashed), 25 (solid), and 28 (dotted-dashed). The folding real potential of the elastic channel with $N_R=1$ (V_{00}) is shown for comparison. The insensitive region shown is for $J=21$.

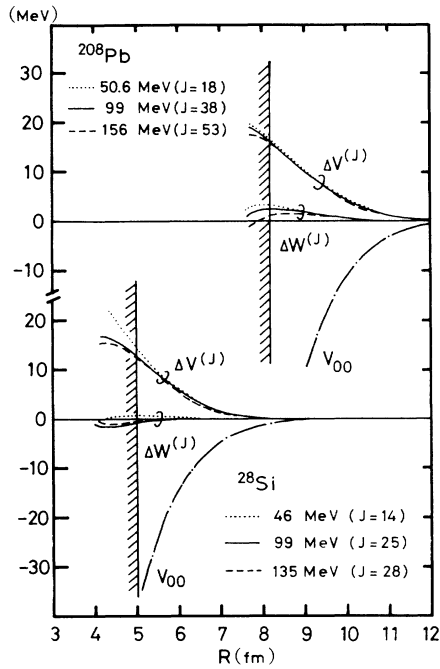


FIG. 10. Bombarding-energy dependence of the DP potential, the real and imaginary parts of which are shown in the case of the ^{208}Pb target (upper) for $E_{\text{lab}} = 50.6, 99,$ and 156 MeV, and in the case of the ^{28}Si target (lower) for $46, 99,$ and 135 MeV. The folding real potentials of the elastic channel with $N_R = 1,$ (V_{00}) are shown for comparison.

and for the scattering by ^{208}Pb at $E_{\text{lab}} = 50.6, 99,$ and 156 MeV. For both targets, the potential changes slightly as the incident energy changes, which explains well the fact that the renormalization factor of $N_R = 0.5-0.6$ occurs almost independently of energy in the single-channel DF-model studies of ^6Li scattering.¹⁰⁻¹⁶

Next we examine the dependence of the DP potential on target nucleus. We calculate the potential for $^{12}\text{C}, ^{28}\text{Si}, ^{40}\text{Ca}, ^{58}\text{Ni},$ and ^{208}Pb targets at an incident energy of $E_{\text{lab}} = 99$ MeV, which corresponds to the CDCC calculation shown in Fig. 5. J has been chosen again to be the one around J_{gr} for each target; note that J_{gr} is 15, 23, 26, 30, and 38 for $^{12}\text{C}, ^{28}\text{Si}, ^{40}\text{Ca}, ^{58}\text{Ni},$ and ^{208}Pb targets, respectively. The solid and dashed lines in Fig. 11 show the real and imaginary parts, respectively, of the DP potential for those targets. For comparison, the real DF potentials in the elastic channel are also shown by the dotted lines. For the cases of $^{28}\text{Si}, ^{40}\text{Ca}, ^{58}\text{Ni},$ and ^{208}Pb targets, the potentials are similar to each other, which satisfies approximately the relationships of $\Delta V^{(J)}(R) \simeq -0.4V_{00}(R)$ and $\Delta W^{(J)}(R) \simeq 0$ in the peripheral region. This result is consistent with the target independence of the renormalization factor $N_R = 0.5-0.6$ required in the DF-model studies.¹⁰⁻¹⁶ For ^{12}C , however, the ratio of $-\Delta V^{(J)}(R)/V_{00}(R)$ is about $0.2-0.3$, which is somewhat smaller than that for other targets, whereas a weak but non-negligible imaginary part of absorptive nature, $\Delta W^{(J)}(R) < 0$, is induced. The exceptional nature of the potential for ^{12}C may have some relation to the neglect of

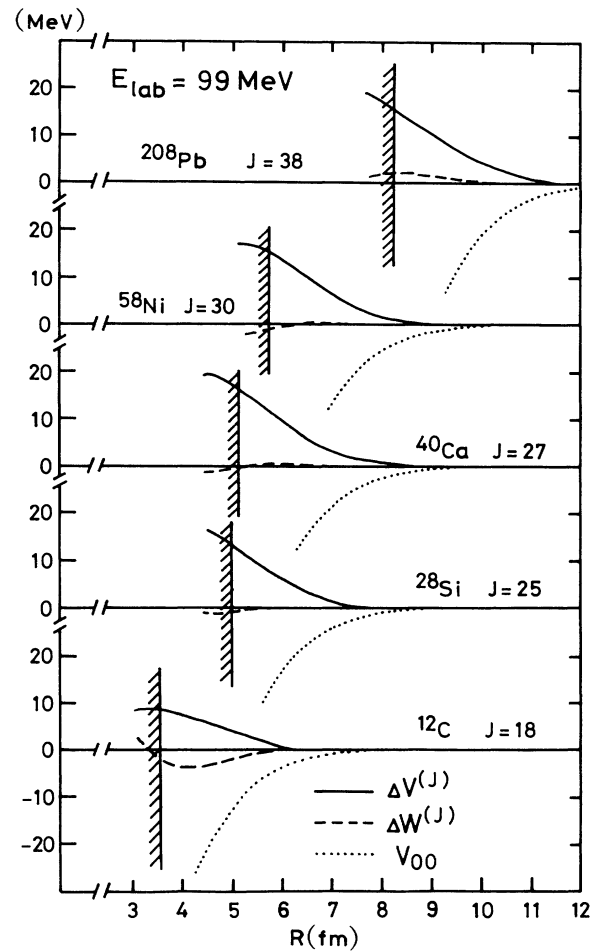


FIG. 11. Target-nucleus dependence of the DP potential. The solid (dashed) lines show the real (imaginary) part of the potential in the case of $^{208}\text{Pb}, ^{58}\text{Ni}, ^{40}\text{Ca}, ^{28}\text{Si},$ and ^{12}C targets from top to bottom. The folding real potentials of the elastic channel are also shown by the dotted lines.

the strong coupling to the target (^{12}C) excitation in the present CDCC calculation, and seems to correlate with the fact that, for ^{12}C , the optimum value of N_I for the CDCC calculation is somewhat smaller (≤ 0.5) than that for the other targets (≥ 0.6), as seen in Table I. In fact, as we will see below, the qualitative feature of the DP potential largely depends on the strength of *imaginary coupling potentials*.

C. Effects of imaginary part of coupling potentials

All the coupling potentials, as well as the diagonal ones, are complex in the present CDCC framework [cf. Eq. (2.13)]. It should be emphasized that the successful results of the CDCC calculation shown in Figs. 2-7 have been achieved by using complex coupling potentials with $N_R = 1.0$ and $N_I \simeq 0.6$. If we switch off the imaginary part of the coupling potentials in the calculation, we cannot reproduce experimental data at all. In order to demonstrate the important role of the imaginary part of the coupling potentials, we compare in Fig. 12 two kinds

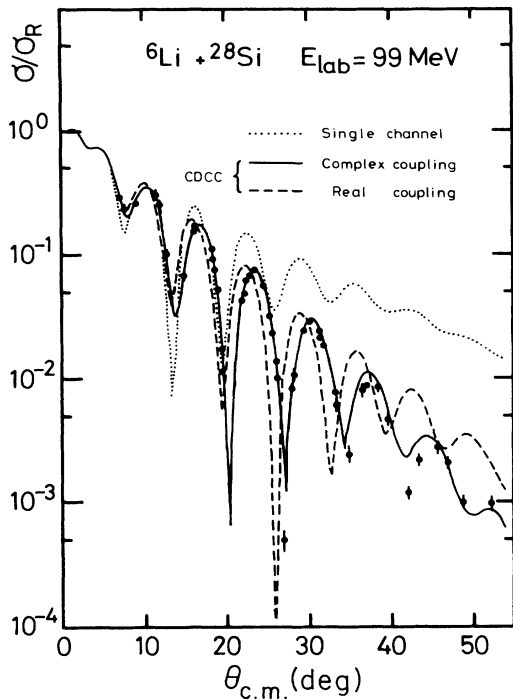


FIG. 12. Angular distribution of ${}^6\text{Li} + {}^{28}\text{Si}$ scattering at 99 MeV; the solid (dashed) line is given by the CDCC calculation with complex (real) coupling potentials with $N_R=1.0$ and $N_I=0.62$ ($N_R=0.0$). Diagonal potentials of all the channels are taken to be complex by keeping $N_R=1.0$ and $N_I=0.62$ in both calculations. The dotted line is the result of the single-channel calculation.

of CDCC calculations for the ${}^6\text{Li} + {}^{28}\text{Si}$ scattering at 99 MeV, one with real coupling potentials ($N_R=1.0$ and $N_I=0.0$) and the other with complex ones ($N_R=1.0$ and $N_I=0.62$). In both calculations all the diagonal potentials are set to be complex with $N_R=1.0$ and $N_I=0.62$. It is obvious from the comparison that the complex coupling potentials with $N_I \approx 0.6$ are indispensable for proper fitting to the data; no matter how widely we changed the value of N_I for the diagonal potentials, no satisfactory fit was obtained as long as we used real coupling potentials alone. Thus, we see that the imaginary part of the coupling potentials is very important in considering the effects of ${}^6\text{Li}$ -breakup channels. A similar importance of the imaginary coupling potentials has been found recently in Ref. 6 for ${}^7\text{Li}$ scattering by ${}^{40}\text{Ca}$ at 89 MeV.

These results suggest that the imaginary part of the coupling potentials is closely related to the qualitative features of the DP potential. This is indeed confirmed in Fig. 13, which shows the DP potentials corresponding to the two kinds of CDCC calculations given in Fig. 12. The switching off of the imaginary part of the coupling potentials causes an essential difference in the qualitative feature of the DP potential; the strength of the repulsive real part ($\Delta V > 0$) has been much reduced, while a considerable absorptive imaginary part ($\Delta W < 0$) has grown, which can hardly account for the empirical renormalization ($\sim 40\%$) to the real folding potential. Thus, for a

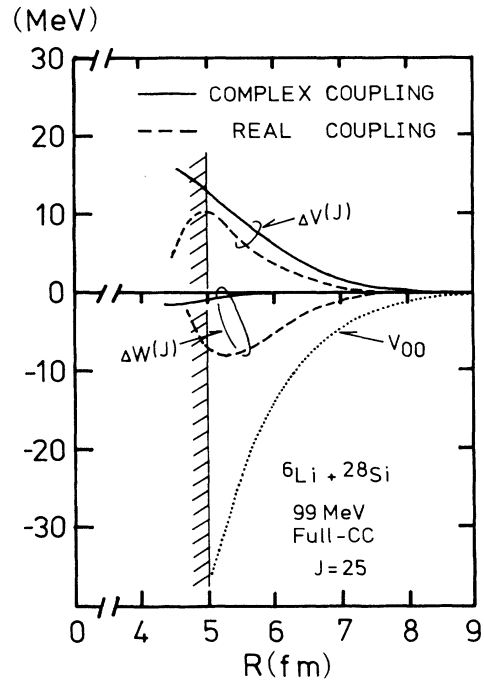


FIG. 13. The real and imaginary parts of the DP potentials given by the CDCC calculation with complex coupling potentials (solid lines) and with real coupling potentials (dashed lines) for $J=25$ of ${}^6\text{Li} + {}^{28}\text{Si}$ scattering at 99 MeV. The real folding potential of the elastic channel is also shown by the dotted line.

proper estimation of ${}^6\text{Li}$ breakup effects, it is quite important to use complex coupling potentials with a considerable amount of the imaginary part.

As shown above, the essential feature of the DP potential is very sensitive to the real-to-imaginary ratio of the complex potential. In the present CDCC framework, we have determined the ratio (i.e., N_I/N_R with N_R kept fixed at unity) phenomenologically in such a way that the CDCC calculation reproduces the observed elastic scattering. Through the CDCC analyses in this paper, experimental data tell us that N_I must be 0.5–0.6 almost independently of the incident energy and target nucleus (cf. Table I). This implies that the DP potential of ${}^6\text{Li}$ breakup depends slightly on the energy and target, having a repulsive real part ($\Delta V \approx -0.4V_{00}$) and a negligible imaginary part ($\Delta W \approx 0$). This result is absolutely consistent with the result of the single-channel DF-model studies^{10–16} that the real part of the empirical ${}^6\text{Li}$ -nucleus potential is systematically shallower in the surface region than the DF model potential by about 40–50%, irrespective of bombarding energy and target nucleus.

V. DISCUSSION

Finally, we try to answer the following questions: Why the qualitative feature of the DP potential is sensitive to the imaginary part of the coupling potentials, and why such a special type of DP potential is generated by the coupling of the breakup process?

A basic role of imaginary coupling on DP potential

may easily be understood by the following consideration. In general, the DP potential can be written symbolically as

$$\Delta U = \sum_{j \neq 0} U_{0j} G_j^{(+)} U_{j0}, \quad (5.1)$$

where $G_j^{(+)}$ is a Green's function in the j th channel. U_{0j} is the complex coupling potential between the incident channel ($i=0$) and the j th channel, which in the present framework is given by $U_{0j} = (N_R + iN_I)V_{0j}$, V_{0j} being the real coupling potential. Hence, Eq. (5.1) is rewritten as

$$\Delta U = (N_R + iN_I)^2 \left[\sum_{j \neq 0} V_{0j} G_j^{(+)} V_{j0} \right]. \quad (5.2)$$

Now we define a DP potential induced by the real coupling potential (V_{0j}) by

$$\Delta u = \Delta v + i \Delta w = \sum_{j \neq 0} V_{0j} G_j^{(+)} V_{j0}, \quad (5.3)$$

where Δv and Δw are the real and imaginary parts, respectively. Then, the real and imaginary parts of ΔU , say, ΔV and ΔW , respectively, are written as

$$\Delta V = [(N_R^2 - N_I^2)\Delta v - 2N_R N_I \Delta w], \quad (5.4a)$$

$$\Delta W = [(N_R^2 - N_I^2)\Delta w + 2N_R N_I \Delta v]. \quad (5.4b)$$

Precisely speaking, Δu itself also depends on the complex factor $N_R + iN_I$ implicitly through $G_j^{(+)}$, because the multistep transitions among nonelastic channels are caused by $U_{ij} = (N_R + iN_I)V_{ij}$, not by V_{ij} . When the multistep transitions are less important, Δu may be weakly dependent on N_R and N_I and, as a result, ΔU depends on them only through the factor of $(N_R + iN_I)^2$ in Eq. (5.2); i.e., the (N_R, N_I) dependence of ΔV and ΔW is given explicitly by Eqs. (5.4a) and (5.4b), respectively (since our interest here is the effect of the complexity of the coupling potentials, not of the diagonal ones; hence, in the present discussion, N_R and N_I for the latter are regarded to be fixed at some realistic values, such as $N_R=1$ and $N_I=0.6$.)

As is well known,⁴² if the coupling among nonelastic channels is negligible (i.e., second-order perturbation theory is valid), the potential Δu is almost pure imaginary with an absorptive nature; namely, $\Delta v \simeq 0$ and $\Delta w < 0$. In such a case, we can discuss the qualitative features of ΔV and ΔW through the ratio of $\alpha = N_I/N_R$ in the following limiting cases:

(i) In the case of real coupling alone, i.e., $\alpha=0$ ($N_I=0$), the DP potential of "conventional type" is induced,

$$\Delta V = 0, \quad \Delta W = N_R^2 \Delta w < 0. \quad (5.5)$$

(ii) In the case of a strong-imaginary coupling such as $\alpha=1$ ($N_I=N_R$),

$$\Delta V = -2N_R^2 \Delta w > 0, \quad \Delta W = 0, \quad (5.6)$$

which is just the type seen in the case of ${}^6\text{Li}$ breakup. The meaning of these results becomes clear if one rewrites Eqs.

(5.4a) and (5.4b) (in the case of $\Delta v=0$) in the form

$$\Delta U = |\Delta U| e^{i\delta}, \quad (5.7)$$

where $|\Delta U| = N_R^2(1+\alpha^2)|\Delta w|$ and $\tan\delta = (\alpha^2-1)/2\alpha$. That is, the ratio α of the imaginary coupling to the real one essentially determines the phase δ of the complex DP potential. This is an answer to the first question mentioned above.

In the second-order perturbation theory, the " ${}^6\text{Li}$ -type" DP potential ($\Delta V > 0$, $\Delta W \simeq 0$) has been realized for $\alpha=1$ [see Eq. (5.6)], while this type of the potential has been generated with $\alpha \simeq 0.6$ in the practical CDCC calculation discussed before. For ${}^6\text{Li}$ breakup, multistep transitions among breakup channels are known to be fairly strong³ and a perturbative treatment of the coupling needs some improvements. Thus in the following we will modify the above assumption, $\Delta v \simeq 0$ and $\Delta w < 0$, so as to include the multistep effects. If the effects are taken into account correctly, Δv in Eq. (5.3) will have a positive value of non-negligible magnitude. In fact, we have already seen in Fig. 13 that a sizable, repulsive potential ($\Delta V > 0$) is generated even when we use the real coupling potentials alone. Here note that Δv and Δw are nothing but ΔV and ΔW themselves, respectively, in the case of $N_R=1$ and $N_I=0$ in Eqs. (5.4). Since Δv and Δw are of opposite sign with each other (cf. Fig. 13), ΔW in Eq. (5.4b) will approximately vanish for a value of N_I between zero and unity, it being about 0.6 in the actual case (cf. Table I and Figs. 9–11). On the other hand, ΔV remains positive for the value of $N_I \simeq 0.6$ since Δv and Δw are of opposite sign. It is due to this mechanism that the DP potential induced by the ${}^6\text{Li}$ -breakup process has a particular property ($\Delta V > 0$, $\Delta W \simeq 0$) with $N_R=1.0$ and $N_I \simeq 0.6$. This is an answer to the second question mentioned above. These properties of the DP potential induced by the breakup channels have been suggested preliminarily in Ref. 43 in the two-channel model, but no *explicit* relationships between ΔU and N_R or N_I , like Eqs. (5.4a) and (5.4b), have been discussed there.

Finally, we emphasize that application of the above discussion should not be limited to the case of ${}^6\text{Li}$ breakup. The basic role of the imaginary part in coupling potentials is quite general as far as we stand on the present CDCC framework. Recently, Kamimura and the present author have reported⁴⁴ that, in the collisions of ${}^{12}\text{C}$ with ${}^{16}\text{O}$ and ${}^{13}\text{C}$ at $E_{\text{lab}}/A_p \simeq 10\text{--}20$ MeV, the repulsive DP potentials similar to the ${}^6\text{Li}$ case are really induced by the coupling with the ${}^{12}\text{C}$ excited states (including ${}^{12}\text{C} \rightarrow 3\alpha$ breakup channels), where the DP potential depends seriously on the incident energy in this case, since the value of N_I increases with the incident energy. Such properties of the DP potential can be reasonably understood from the consideration discussed above. This will be given elsewhere.⁴⁵

VI. SUMMARY AND CONCLUSION

In this paper we have investigated the ${}^6\text{Li} \rightarrow \alpha + d$ virtual breakup effect on elastic scattering of ${}^6\text{Li}$ over a wide range of bombarding energy ($E_{\text{lab}} = 34\text{--}169$ MeV) and for many target nuclei (${}^{12}\text{C}$, ${}^{28}\text{Si}$, ${}^{40}\text{Ca}$, ${}^{48}\text{Ca}$, ${}^{58}\text{Ni}$, and ${}^{208}\text{Pb}$),

which almost covers the energies and targets of currently available data for elastic scattering of ${}^6\text{Li}$. The breakup process is treated by the method of coupled discretized continuum channels (CDCC), in which the breakup states in the α -d S wave ($l=0$), P wave ($l=1$), and D wave ($l=2$) with α -d relative momentum up to $k=1.5\text{ fm}^{-1}$ are taken into account (Fig. 1). The internal wave function of ${}^6\text{Li}$ in the ground state as well as those in the breakup continuum states are calculated on the basis of microscopic α -d cluster model. Projectile-target diagonal potentials as well as coupling interactions which generate projectile excitations are given by the folding of M3Y NN interaction with nucleon density distributions of colliding nuclei. The calculation reproduces well the measured cross sections for all the targets and bombarding energies (Figs. 2–7) without imposing any reduction factor to the real DF potential, i.e., keeping N_R at unity. The breakup effects are very large and are essential to reproduce the observed elastic scattering data; when the couplings with the breakup channels are omitted, there is no way to reproduce the observed cross section as long as $N_R=1$ persists. Furthermore, it is shown that the dynamical polarization (DP) potential induced by the coupling with the breakup channels is a repulsive potential which cancels about 40% of the attractive folding potential in the nuclear surface region. These results provide evidence that the breakup effect is the real origin of the renormalization factor $N_R=0.5\text{--}0.6$ in the single-channel DF-model analyses of the elastic scattering. Since the renormalization factor in the DF model was found to be almost constant ($N_R=0.5\text{--}0.6$) for the energies and targets investigated so far, this also implies that the breakup effect is almost independent of bombarding energy and target nucleus. In fact, this is directly confirmed by the calculated DP potential (Figs. 9–11), the essential properties of which ($\Delta V \simeq -0.4V_{00}$ and $\Delta W \simeq 0$) are shown to be almost independent of bombarding energy and target nucleus as well as of angular momentum. As shown in Figs.

12 and 13, the calculated results are quite sensitive to the strength of imaginary coupling potentials, and reasonable agreement with the data require the values of $N_I=0.5\text{--}0.6$ (see Table I) almost independently of energy and target. These features can be understood qualitatively by the perturbation-theoretic consideration. Thus, in some sense the present analyses provide a justification for the phenomenological determination of the imaginary interaction, giving information about basic interactions of ${}^6\text{Li}$ -nucleus systems in the present bombarding energy region. Further fundamental justifications can be obtained by more microscopic treatment of the imaginary part of internucleus interactions. In particular, it may be challenging to investigate whether microscopic coupled-channel theories⁴⁶ such as those based on the nuclear matter approach for internucleus interactions are able to reproduce the energy and target independences of basic interactions that have been found phenomenologically in the present work. Further experimental investigations for ${}^6\text{Li}$ -nucleus scattering, as well as those for other heavy ion systems, are also desirable at much higher energy regions. Also, polarization phenomena will provide more information for the ${}^6\text{Li}$ -nucleus interaction.^{8,9}

ACKNOWLEDGMENTS

The author would like to thank Dr. M. Kamimura and Dr. M. Yahiro for stimulating discussion and Prof. M. Muraoka for continuous encouragement. He is also grateful to Prof. M. Tanifuji for careful reading of the manuscript. A computer code for nearside/farside decomposition has been provided by Dr. Y. Iseri and Mr. A. Fujiyama. Financial support of the Japan Society for the Promotion of Science is gratefully acknowledged. Numerical calculations were done with the FACOMM380 computer at the Institute for Nuclear Study, University of Tokyo.

*Present address: Department of Physics, Osaka City University, Sumiyoshi-ku, Osaka 558, Japan.

¹I. J. Thompson and M. A. Nagarajan, Phys. Lett. **106B**, 163 (1981).

²Y. Sakuragi, M. Yahiro, and M. Kamimura, Prog. Theor. Phys. **68**, 322 (1982).

³Y. Sakuragi, M. Yahiro, and M. Kamimura, Prog. Theor. Phys. **70**, 1047 (1983).

⁴M. A. Nagarajan, I. J. Thompson, and R. C. Johnson, Nucl. Phys. **A385**, 525 (1982).

⁵Y. Sakuragi, M. Yahiro, and M. Kamimura, in Proceedings of the 1983 RCNP International Symposium on Light Ion Reaction Mechanism (Contributed Papers), Osaka, 1983, edited by H. Ogata, T. Kammuri, and I. Katayama (unpublished), p. 84.

⁶J. Gomez-Camacho, M. Lozano, and M. A. Nagarajan, Nucl. Phys. **A440**, 543 (1985).

⁷J. Gomez-Camacho, M. Lozano, and M. A. Nagarajan, Phys.

Lett. **161B**, 39 (1985).

⁸H. Nishioka, R. C. Johnson, J. A. Tostevin, and K.-I. Kubo, Phys. Rev. Lett. **48**, 1795 (1982); H. Nishioka, J. A. Tostevin, and R. C. Johnson, Phys. Lett. **124B**, 17 (1983); H. Nishioka, J. A. Tostevin, R. C. Johnson, and K.-I. Kubo, Nucl. Phys. **A415**, 230 (1984); G. Windham, H. Nishioka, J. A. Tostevin, and R. C. Johnson, Phys. Lett. **138B**, 253 (1984); H. Nishioka and R. C. Johnson, Phys. Rev. Lett. **53**, 1881 (1984); H. Nishioka and R. C. Johnson, Nucl. Phys. **A440**, 557 (1985).

⁹H. Ohnishi, M. Tanifuji, M. Kamimura, and M. Yahiro, Phys. Lett. **118B**, 16 (1982); H. Ohnishi, M. Tanifuji, M. Kamimura, Y. Sakuragi, and M. Yahiro, Nucl. Phys. **A415**, 271 (1984); Y. Sakuragi, M. Kamimura, M. Yahiro, and M. Tanifuji, Phys. Lett. **153B**, 372 (1985); M. Kamimura, Y. Sakuragi, M. Yahiro, and M. Tanifuji, in Proceedings of the Sixth International Symposium on Polarization Phenomena in Nuclear Physics, Osaka, 1985, edited by M. Kondo, S. Kobayashi, M. Tanifuji, T. Yamazaki, K.-I. Kubo, and N.

- Ohnishi [J. Phys. Soc. Jpn. **55** Suppl., 205 (1986)]; T. Sakuragi, M. Kamimura, M. Yahiro, and M. Tanifuji, Phys. Lett. **175B**, 105 (1986); Y. Sakuragi, M. Yahiro, M. Kamimura, and M. Tanifuji, Nucl. Phys. **A462**, 173 (1987).
- ¹⁰G. R. Satchler and W. G. Love, Phys. Rep. **55**, 183 (1979).
- ¹¹D. P. Stanley, F. Petrovich, and P. Schwandt, Phys. Rev. C **22**, 1375 (1980).
- ¹²G. R. Satchler and W. G. Love, Phys. Lett. **76B**, 23 (1978); G. R. Satchler, Nucl. Phys. **A329**, 233 (1979).
- ¹³J. Cook, Nucl. Phys. **A375**, 238 (1982).
- ¹⁴C. W. Glover, R. I. Cutler, and K. W. Kemper, Nucl. Phys. **A341**, 137 (1980).
- ¹⁵M. F. Steeden, J. Coopersmith, S. J. Cartwright, M. D. Cohler, N. M. Clarke, and R. J. Griffiths, J. Phys. G **6**, 501 (1980).
- ¹⁶J. Cook, N. M. Clarke, and R. J. Griffiths, Nucl. Phys. **A357**, 246 (1981).
- ¹⁷G. Bertsch, J. Borysowicz, H. McManaus, and W. G. Love, Nucl. Phys. **A284**, 399 (1977).
- ¹⁸R. S. Mackintosh and A. M. Kobos, Phys. Lett. **116B**, 95 (1982); A. A. Ioannides and R. S. Mackintosh, *ibid.* **169B**, 113 (1986).
- ¹⁹H. Amakawa, A. Mori, H. Nishioka, K. Yazaki, and S. Yamaji, Phys. Rev. C **23**, 583 (1981).
- ²⁰G. H. Rawitscher, Phys. Rev. C **9**, 2210 (1974); **11**, 1152 (1975); G. H. Rawitscher, Nucl. Phys. **A241**, 365 (1975).
- ²¹J. P. Farrel, Jr., C. M. Vincent, and N. Austern, Ann. Phys. (N.Y.) **96**, 333 (1976); N. Austern, C. M. Vincent, and J. P. Farrel, Jr., *ibid.* **114**, 93 (1978).
- ²²M. Yahiro and M. Kamimura, Prog. Theor. Phys. **65**, 2046 (1981); **65**, 2051 (1981).
- ²³M. Yahiro, M. Nakano, Y. Iseri, and M. Kamimura, Prog. Theor. Phys. **67**, 1467 (1982).
- ²⁴S. Saito, Prog. Theor. Phys. **41**, 705 (1969); T. Matsuse and M. Kamimura, *ibid.* **49**, 1765 (1973).
- ²⁵J. A. Wheeler, Phys. Rev. **52**, 1083 (1937).
- ²⁶G. C. Li, I. Sick, R. R. Whitney, and M. R. Yearian, Nucl. Phys. **A162**, 583 (1971); R. Yen, L. S. Cardman, D. Kalinsky, J. R. Legg, and C. K. Bockelman, *ibid.* **A235**, 135 (1974).
- ²⁷J. W. Negele, Phys. Rev. C **1**, 1260 (1970).
- ²⁸M. Kamimura, Nucl. Phys. **A351**, 456 (1981).
- ²⁹K. Katori, T. Shimoda, T. Fukuda, S. Shimoura, A. Sakaguchi, M. Tanaka, T. Yamagata, N. Takahashi, H. Ogata, Y. Sakuragi, and M. Kamimura (submitted to Nucl. Phys. A).
- ³⁰R. I. Cutler, M. J. Nadworny, and K. W. Kemper, Phys. Rev. C **15**, 1318 (1977).
- ³¹H. Gemmeke, B. Deluigi, L. Lassen, and D. Scholz, Z. Phys. A **286**, 73 (1978).
- ³²L. I. Chua, F. D. Becchetti, J. Janecke, and F. L. Mildner, Nucl. Phys. **A273**, 243 (1976).
- ³³C. B. Fulmer, G. R. Satchler, E. E. Gross, F. E. Bertrand, C. D. Goodman, D. C. Hensley, and J. R. Wu, Nucl. Phys. **A356**, 235 (1981).
- ³⁴R. Huffman, A. Galonsky, R. Markham, and C. Williamson, Phys. Rev. C **22**, 1522 (1980).
- ³⁵R. M. DeVries, D. A. Goldberg, J. W. Watson, M. S. Zisman, and J. G. Cramer, Phys. Rev. Lett. **39**, 450 (1977).
- ³⁶P. Schwandt, S. Kailas, W. W. Jacobs, M. D. Kaitchuch, W. Ploughe, and P. P. Singh, Phys. Rev. C **21**, 1656 (1980).
- ³⁷Z. Majka, H. J. Gils, and H. Rebel, Z. Phys. A **288**, 139 (1978).
- ³⁸J. Cook, H. J. Gils, H. Rebel, Z. Majka, and H. Klewe-Nebenius, Nucl. Phys. **A388**, 173 (1982).
- ³⁹J. Cook, Nucl. Phys. **A388**, 153 (1982).
- ⁴⁰R. C. Fuller, Phys. Rev. C **12**, 1561 (1975).
- ⁴¹K. W. McVoy and G. R. Satchler, Nucl. Phys. **A417**, 157 (1984); G. R. Satchler, *Direct Nuclear Reactions* (Clarendon, Oxford, New York, 1983).
- ⁴²W. G. Love, T. Terasawa, and G. R. Satchler, Nucl. Phys. **A291**, 183 (1977); K.-I. Kubo and P. E. Hodgson, *ibid.* **A366**, 320 (1981).
- ⁴³M. Kamimura, M. Yahiro, Y. Iseri, M. Nakano, and Y. Sakuragi, in *Clustering Aspects of Nuclear Structure*, edited by J. S. Lilley and M. A. Nagarajan (Reidel, Dordrecht, 1985).
- ⁴⁴Y. Sakuragi and M. Kamimura, Phys. Lett. **149B**, 307 (1984).
- ⁴⁵Y. Sakuragi, M. Yahiro, and M. Kamimura, Prog. Theor. Phys. Suppl. **89**, 136 (1986).
- ⁴⁶A. Faessler, W. H. Dickhoff, M. Trefz, and M. Rhoades-Brown, Nucl. Phys. **A428**, 271c (1984); M. Trefz, A. Faessler, W. H. Dickhoff, and M. Rhoades-Brown, Phys. Lett. **149B**, 459 (1984).